Control Engineering Practice 53 (2016) 35–46

Contents lists available at ScienceDirect

Control Engineering Practice

journal homepage: www.elsevier.com/locate/conengprac

Current-sensor fault detection and isolation for induction-motor drives using a geometric approach

F. Aguilera [a,*], P.M. de la Barrera [a], C.H. De Angelo [a], D.R. Espinoza Trejo [b]

[a] Grupo de Electrónica Aplicada, Universidad Nacional de Río Cuarto, CONICET, Argentina
[b] Coordinación Académica Región Altiplano, Universidad Autónoma de San Luis Potosí, Mexico

ARTICLE INFO

Article history:
Received 19 July 2015
Received in revised form
19 April 2016
Accepted 21 April 2016

Keywords:
Induction motor drive
Fault detection and isolation
Nonlinear observer
Sensor
Geometric approach

ABSTRACT

This work presents the design of a current-sensor fault detection and isolation system for induction-motor drives. A differential geometric approach is addressed to determine if faults can be detected and isolated in drives with two line current sensors by using a model based strategy. A set of subsystems is obtained based on the observability co-distribution, whose outputs are decoupled from the load torque (detectability) and only affected by one of the sensors (isolability). A bank of observers is designed for these subsystems in order to obtain residuals for the fault detection and isolation. It is demonstrated that the proposed strategy allows detecting single and multiple sensor faults, including disconnection, offset and gain faults. Experimental results validate the proposal.

1. Introduction

Induction motors (IM) are widely used for servo systems in applications where a high performance speed or torque control is required, such as industry automation and traction systems. Faults in some components of IM drives (IMD) (motor, power electronics, driving circuits, sensors) can degrade the overall system performance, damage its internal components or leave it out of operation. Moreover, in many applications IMD are used in critical systems, where faults can endanger the safety of persons (Aguilera, de la Barrera, & De Angelo, 2012; Giantomassi, Ferracuti, Iarlori, Ippoliti, & Longhi, 2015; Raisemche, Boukhnifer, Larouci, & Diallo, 2014). For this reason, in last years the study of fault detection and isolation systems (FDIS) for IMD has been an important topic in different scientific publications (Arnanz, Miguel, Perán, & Mendoza, 2011; Drobnič, Nemec, Fišer, & Ambrožič, 2012; Mustafa, Nikolakopoulos, Gustafsson, & Kominiak, 2016; Pons-Llinares et al., 2015; Riera-Guasp, Antonino-Daviu, & Capolino, 2015; Zhang, Zhao, Zhou, & Huang, 2014). These systems are used to report the occurrence of a fault and to determine which components are affected, in order to avoid problems caused by faults. In this way, the information provided by the FDIS can be used by a fault tolerant drive (FTD), where a control reconfiguration mechanism enables to keep the IMD in operation despite the fault (Fonod et al., 2015; Marino, Scalzi, Tomei, & Verrelli, 2013; Schuh, Zgorzelski, & Lunze, 2015; Shi & Krishnamurthy, 2014).

In particular, faults in the feedback sensors can produce critical consequences in the IMD performance. As it was shown in Aguilera et al. (2012), a current-sensor fault produces very high current values in the IM phases in a short period of time. Therefore, this fact must be taken into account in order to develop and design the fault detection stage in a FTD for current sensors. Mechanical speed or position sensors are more prone to faults than current sensors. Nevertheless, its effect over phase currents is not so serious, requiring longer times for its detection (Aguilera et al., 2012). In addition, the design of FDIS for mechanical sensors have been widely threated in literature and have proved to give good results (Kommuri, Rath, Veluvolu, Defoort, & Soh, 2015; Raisemche et al., 2014). Therefore, it is necessary to study further the design of fast FDIS for current sensors.

Most fault detection methods for current sensors proposed in literature are based on physical redundancy by using three line current sensors in the IMD (Shi & Krishnamurthy, 2014; Freire et al., 2014; Yu et al., 2014). Nevertheless, the use of redundant sensors increases the system size and costs (Zhang et al., 2013). For this reason, some works propose FDIS using only the information of two line current sensors. For example, in Najafabadi, Salmasi, and Jabehdar-Maralani (2011) an adaptive observer is proposed for

* Corresponding author.
E-mail addresses: faguilera@ing.unrc.edu.ar (F. Aguilera), pbarrera@ing.unrc.edu.ar (P.M. de la Barrera), cdeangelo@ing.unrc.edu.ar (C.H. De Angelo), espinoza_trejo_dr@uaslp.mx (D.R. Espinoza Trejo).

http://dx.doi.org/10.1016/j.conengprac.2016.04.014
0967-0661/

detecting faults in current, speed or voltage sensors. This technique is based on the assumption that only one sensor may be faulty at a time, namely, only single faults can be isolated. This approach requires to compute the average value of residuals along some electrical cycles, which implies a long time for fault isolation.

A similar method for fault detection and isolation of single sensor faults has been reported in Zhang et al. (2013). The fault detection and isolation is performed by computing residuals from a Kalman filter and the absolute values of the currents. These residuals are not perfectly decoupled from each other, and therefore thresholds must be carefully selected, by following empirical algorithms. This approach is not able to detect the recovery of a sensor from a faulty condition, for example, after a short duration fault.

In Chakraborty and Verma (2015), a FDIS for speed and current-sensor faults based on axes transformations is proposed. Residuals used for the detection of current-sensor faults depend on the reference currents used for the control strategy. These residuals are affected by current tracking errors and faults in the current sensors, therefore it is difficult to distinguish between them when residuals are evaluated. This fact is the main drawback of the cited method. Another drawback is the inability of diagnosing the recovery of a sensor from a fault.

Only disconnection faults were considered in all the previous cited works. In addition, the theoretical analysis for obtaining residuals sensitive to faults in a specific current sensor and decoupled from load variations was not addressed. A comparison of the previous cited FDIS for current sensors is summarized in Table 1.

As it can be seen from cited works, there are few studies on single and multiple current-sensor fault detection and isolation in IMD using only two current sensors. Hence, the main objective of the present work is to propose a method to design a FDIS considering multiple current-sensor faults without physical redundancy. For this purpose, the fundamental problem of residual generation (FPRG) for nonlinear systems is first studied for IMD with current sensors faults (De Persis & Isidori, 2001). This approach proposes geometrical conditions in order to determine if a specific fault can be decoupled from other faults and perturbations. If these conditions are satisfied, then a coordinates transformation can be obtained. This transformation allows to obtain a subsystem whose output is sensitive to that specific fault. If several faults are considered in this analysis, a set of subsystems can be obtained. Then, dedicated residual signals can be designed using a state observer deduced from these subsystems.

The geometric approach was previously applied to IMD addressing different types of faults, such as actuator (Espinoza-Trejo & Campos-Delgado, 2009) and stator short-circuit faults (Khelouat, Benalia, Boukhetala, & Laleg-Kirati, 2012). These works show the usefulness of the approach in order to design diagnostic systems in this application. In this paper, the FPRG is analyzed using a model of the IM considering current sensors faults as arbitrary inputs and the load torque as a perturbation. Based on this model, two new representations of the IM in stationary reference frames are obtained. These representations are used for designing a bank of observers in order to generate dedicated residuals to develop the FDIS.

With the proposed FDIS, the following main technical contributions were achieved (see Table 1):

- Single and multiple current sensor fault detection and isolation are performed without sensor redundancy.
- The FDIS is sensitive to different kind of faults, such as disconnection, offset and gain errors.
- Residuals are sensitive to the fault derivative, allowing an early detection of sudden faults.

Table 1
Comparison of different current-sensor FDIS for IMD.

Reference	Fault detection method	Required measurements[a]	Considered kind of faults	Detection and isolation of single and multiple faults	Independent of the control strategy	Fault detection time	Recovery from a faulty condition
Shi and Krishnamurthy (2014)	Redundant sensor	3 currents	Disconnection	Only detection	Yes	Not reported	Yes
Freire, Estima, and Cardoso (2014)[b]	Redundant sensor	3 currents	Disconnection	Only single faults	Yes	5 ms	Yes
Yu, Wang, Xu, Zhou, and Xu (2014)	Bank of observers	1 voltage, 3 currents, 1 speed	Disconnection	Only single faults	Yes	Not reported	No
Zhang et al. (2013)	EKF	1 voltage, 2 currents, 1 speed	Disconnection	Only single faults	Yes	Not reported	No
Najafabadi et al. (2011)	Adaptive observer	1 voltage, 2 currents, 1 speed	Disconnection	Only single faults	Yes	300 ms	Yes
Chakraborty and Verma (2015)	Analysis of current tracking errors	1 voltage, 2 currents, 1 speed[c]	Disconnection	Yes	No	Not reported	No
This work	Bank of observers	1 voltage, 2 currents, 1 speed	Disconnection, offset, gain	Yes	Yes	1 ms	Yes

[a] Generally, stator voltages are approximated based on the inverter switches command signals and a single DC-link voltage sensor. In some applications, DC-link voltage is assumed to be known and constant, hence the voltage sensor can be avoided (Najafabadi et al., 2011).
[b] This approach was proposed for permanent-magnet synchronous generators, but it could be applicable to IMD. In addition, this approach assumes that measured currents are sinusoidal.
[c] In this proposal, a rotor speed estimation method based on the control reference currents is used when the speed sensor is under fault.

- The FDIS is not based on the control reference currents, and hence they are not affected by current estimation errors nor the IMD control strategy.
- There is no need of steady-state, open-loop, or special operating condition for fault isolation because residuals are decoupled from load torque.
- The proposed system is able to detect the recovery of a sensor from a faulty condition.

The obtained results can be used in combination with speed or voltage sensors fault detection methods in order to design a comprehensive FDIS for IMD sensors (Chakraborty & Verma, 2015; Kommuri et al., 2015).

The rest of the paper is organized as follows. First, the addressed geometric approach is briefly described in Section 2. In Section 3, the FPRG is studied for IMD considering current-sensor faults and a bank of observers is proposed. Experimental results as well as a parameter variation study are presented to validate the proposed FDIS in Section 4. Finally, conclusions are drawn in Section 5.

2. Differential geometric approach

The differential geometric approach used in this work is briefly described in this section (De Persis & Isidori, 2001). The following nonlinear system with faults is considered:

$$\dot{\mathbf{x}} = \mathbf{g}_0(\mathbf{x}) + \sum_{k=1}^{m^*} \mathbf{g}_k(\mathbf{x})u_k + \mathbf{l}(\mathbf{x})f_i + \sum_{j=1}^{d^*} \boldsymbol{\rho}_j(\mathbf{x})w_j$$
$$\mathbf{y} = \mathbf{h}(\mathbf{x}) \tag{1}$$

where $\mathbf{x} \in \mathbb{R}^n$ is the state vector, $\mathbf{y} \in \mathbb{R}^p$ is the output vector, u_k ($k=1, \ldots, m^*$) are known inputs, $\mathbf{g}_0, \ldots, \mathbf{g}_{m^*}, \boldsymbol{\rho}_1, \ldots, \boldsymbol{\rho}_{d^*}, \mathbf{l}$ and $\mathbf{h}$ are smooth vectorial fields. Signals $w_1, \ldots, w_{d^*}$ represent d^* unknown arbitrary inputs whereas f_i represents the fault signal that must be detected and isolated. Inputs w_j represent perturbations and other fault signals. This representation is obtained by assuming that s^* fault inputs $f_1, \ldots, f_{s^*}$ and t^* perturbations $p_1, \ldots, p_{t^*}$ are considered. Then, set $d^* = t^* + (s^* - 1)$ such that the unknown arbitrary inputs can be obtained as

$$\mathbf{w} = [w_1, w_2, \ldots, w_{d^*}]^\top = \left[p_1, \ldots, p_{t^*}, f_1, \ldots, f_{i-1}, f_{i+1}, \ldots, f_{s^*}\right]^\top.$$

The objective of this approach is to obtain a subsystem with an output vector sensitive to the fault f_i but decoupled from perturbations and other faults. Then, a residual can be designed using a dedicated observer for that subsystem, thus allowing the detection and isolation of fault f_i. According to De Persis and Isidori (2001), let $\mathbf{P}$ be the distribution defined by:

$$\mathbf{P} = \text{span}\{\boldsymbol{\rho}_1, \boldsymbol{\rho}_2, \ldots, \boldsymbol{\rho}_{d^*}\} \tag{2}$$

then, the FPRG has a solution only if

$$\mathbf{l}(\mathbf{x}) \notin \boldsymbol{\Omega}^\perp \tag{3}$$

where $\boldsymbol{\Omega}$ is the largest observability codistribution contained in $\mathbf{P}^\perp$. This observability codistribution can be computed through the algorithms described in De Persis and Isidori (2001).

If condition (3) is satisfied, changes of coordinates in the state and output spaces can be obtained in order to deduce the subsystem. In case that $\boldsymbol{\Omega}$ is independent of state and $\mathbf{h}(\mathbf{x}) = \mathbf{C}\mathbf{x}$, with $\mathbf{C}$ being a constant matrix, it implies that the transformations are linear mappings (Espinoza-Trejo & Campos-Delgado, 2009). The procedure to obtain the changes of coordinates for this class of systems is recalled below.

Let n_1 the dimension of $\boldsymbol{\Omega}$. It is assumed that $\boldsymbol{\Omega}$ is locally spanned by exact differentials and that $\mathbf{h}(\mathbf{x}) = \mathbf{C}\mathbf{x}$ with $\text{span}\{\mathbf{C}\}$ being full row rank. Let $p - n_2$ be the dimension of $\boldsymbol{\Omega} \cap \text{span}\{\mathbf{C}\}$ and assume that there exists a surjection $\mathbf{H}_1$: $\mathbb{R}^p \to \mathbb{R}^{p-n_2}$ such that

$$\boldsymbol{\Omega} \cap \text{span}\{\mathbf{C}\} = \text{span}\{\mathbf{H}_1\mathbf{C}\}. \tag{4}$$

Then, there exists a matrix $\mathbf{H}_2$ such that

$$\boldsymbol{\psi} = \begin{bmatrix} \boldsymbol{\psi}_1 \\ \boldsymbol{\psi}_2 \end{bmatrix} = \mathbf{H}$$
$$\mathbf{y} = \begin{bmatrix} \mathbf{H}_1 \\ \mathbf{H}_2 \end{bmatrix} \mathbf{y} \tag{5}$$

where $\mathbf{H}$ is an isomorphism over $\mathbb{R}^p$ which represents the transformations of the outputs space. Now, choose a matrix $\boldsymbol{\Phi}_1 \in \mathbb{R}^{n_1 \times n}$, such that:

$$\boldsymbol{\Omega} = \text{span}\{\boldsymbol{\Phi}_1\}. \tag{6}$$

Then, there exists a matrix $\boldsymbol{\Phi}_3 \in \mathbb{R}^{n-(n_1+n_2)\times n}$ such that:

$$\mathbf{z} = \begin{bmatrix} \mathbf{z}_1 \\ \mathbf{z}_2 \\ \mathbf{z}_3 \end{bmatrix} = \boldsymbol{\Phi}$$
$$\mathbf{x} = \begin{bmatrix} \boldsymbol{\Phi}_1 \\ \mathbf{H}_2\mathbf{C} \\ \boldsymbol{\Phi}_3 \end{bmatrix} \mathbf{x} \tag{7}$$

where $\boldsymbol{\Phi}$ is an invertible matrix which represents the transformation of the states space.

A subsystem with output decoupled from perturbations w_j but affected from the fault f_i is obtained considering $\mathbf{z}_1$ as the state vector and $\boldsymbol{\psi}_2 = \mathbf{z}_2$ as a known input (De Persis & Isidori, 2001).

3. FDIS for current sensor faults in IMD

This work studies the design of a FDIS based on a bank of observers, as illustrated in Fig. 1. It is assumed that a speed control strategy is implemented in the IMD. The control loop uses two line currents, i_a and i_b, which are measured through sensors prone to faults. These faults are modelled by arbitrary signals, m_a and m_b, added to the line currents. The differential geometric approach is used in order to design a bank of observers which generates residuals, ν_a or ν_b, sensitive to the faults. Then, by the post-processing of the residual signals, the detection and isolation of the current sensor faults is performed using two logic signals, F_a and F_b, which indicate the detection of a fault in sensor a or sensor b, respectively.

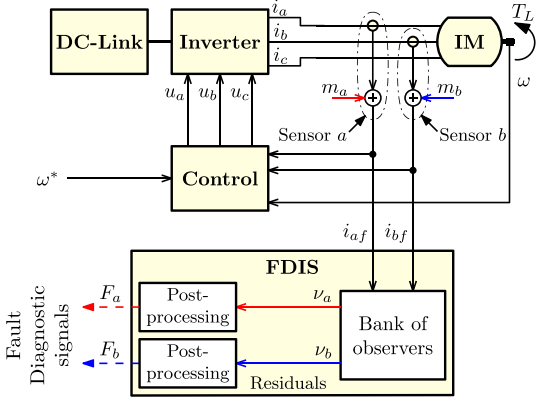

Fig. 1. System under study.

3.1. IM model with current sensor faults

The IM model is described in two stationary reference frames, denoted by (α, β) and $(\tilde{\alpha}, \tilde{\beta})$ (Chakraborty & Verma, 2015). These frames are obtained by linear transformations applied to the three phase electromagnetic variables, denoted by (a, b, c). A graphic representation of the stationary reference frames is shown in Fig. 2, where ζ denotes the components of the currents, voltages or fluxes. It can be observed that in the (α, β) frame, the α component is aligned with axis a, whereas in the $(\tilde{\alpha}, \tilde{\beta})$ frame, the $\tilde{\alpha}$ component is aligned with axis b.

In order to obtain the representation of the IM model in the (α, β) frame, transformation $\left[\zeta_\alpha \ \ \zeta_\beta\right]^\top = \mathbf{T}[\zeta_a \ \ \zeta_b \ \ \zeta_c]^\top$ is used, where

$$\mathbf{T} = \frac{2}{3}\begin{bmatrix} 1 & -\frac{1}{2} & -\frac{1}{2} \\ 0 & \frac{\sqrt{3}}{2} & -\frac{\sqrt{3}}{2} \end{bmatrix}. \tag{8}$$

The IM model is represented in the (α, β) frame by the following dynamic equations:

$$\begin{aligned} \dot{i}_\alpha &= -a i_\alpha + bc\lambda_\alpha + b\omega\lambda_\beta + du_\alpha \\ \dot{i}_\beta &= -a i_\beta + bc\lambda_\beta - b\omega\lambda_\alpha + du_\beta \\ \dot{\lambda}_\alpha &= L_M c i_\alpha - c\lambda_\alpha - \omega\lambda_\beta \\ \dot{\lambda}_\beta &= L_M c i_\beta - c\lambda_\beta + \omega\lambda_\alpha \\ \dot{\omega} &= -kc_f\omega + kc_t(i_\alpha\lambda_\beta - i_\beta\lambda_\alpha) - kT_L \end{aligned} \tag{9}$$

where constants are $a = \frac{L_r^2 R_s + L_M^2 R_r}{\sigma L_r^2}$; $b = \frac{L_M}{\sigma}$; $c = \frac{R_r}{L_r}$; $d = \frac{L_r}{\sigma}$; $\sigma = (L_r L_s - L_M^2)$; $k = \frac{1}{J}$ and $c_t = \frac{PL_M}{L_r}$. R_s and R_r are stator and rotor resistances, respectively; L_s, L_r and L_M are stator, rotor and magnetizing inductances, respectively; J and P are the moment of inertia and the number of pole pairs, respectively; c_f is the friction coefficient; i_α and i_β are stator currents; λ_α and λ_β are rotor fluxes; u_α and u_β are stator voltages; ω is the rotor speed; T_L is the load torque, which is considered as an arbitrary input.

The components in the $(\tilde{\alpha}, \tilde{\beta})$ reference frame are obtained by transformation $\left[\zeta_{\tilde{\alpha}} \ \ \zeta_{\tilde{\beta}}\right]^\top = \tilde{\mathbf{T}}[\zeta_a \ \ \zeta_b \ \ \zeta_c]^\top$, where

$$\tilde{\mathbf{T}} = \frac{2}{3}\begin{bmatrix} -\frac{1}{2} & 1 & -\frac{1}{2} \\ -\frac{\sqrt{3}}{2} & 0 & \frac{\sqrt{3}}{2} \end{bmatrix}. \tag{10}$$

With this transformation, the IM model in the $(\tilde{\alpha}, \tilde{\beta})$ frame is described as:

$$\begin{aligned} \dot{i}_{\tilde{\alpha}} &= -a i_{\tilde{\alpha}} + bc\lambda_{\tilde{\alpha}} + b\omega\lambda_{\tilde{\beta}} + du_{\tilde{\alpha}} \\ \dot{i}_{\tilde{\beta}} &= -a i_{\tilde{\beta}} + bc\lambda_{\tilde{\beta}} - b\omega\lambda_{\tilde{\alpha}} + du_{\tilde{\beta}} \\ \dot{\lambda}_{\tilde{\alpha}} &= L_M c i_{\tilde{\alpha}} - c\lambda_{\tilde{\alpha}} - \omega\lambda_{\tilde{\beta}} \\ \dot{\lambda}_{\tilde{\beta}} &= L_M c i_{\tilde{\beta}} - c\lambda_{\tilde{\beta}} + \omega\lambda_{\tilde{\alpha}} \\ \dot{\omega} &= -kc_f\omega + kc_t(i_{\tilde{\alpha}}\lambda_{\tilde{\beta}} - i_{\tilde{\beta}}\lambda_{\tilde{\alpha}}) - kT_L. \end{aligned} \tag{11}$$

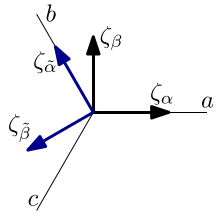

Fig. 2. Graphic representation of the stationary reference frames.

As already mentioned, current sensor faults are modelled as arbitrary inputs m_a and m_b added to line currents, as follows:

$$\begin{aligned} i_{af} &= i_a + m_a \\ i_{bf} &= i_b + m_b \end{aligned} \tag{12}$$

where i_{af} and i_{bf} are the outputs from sensors (see Fig. 1). This modelling of current sensor faults can represent constant or time-varying failures, and they can include offset, gain or disconnection faults. The representations of faults in the previously introduced reference frames is obtained below.

3.1.1. Faults in the (α, β) reference frame

Considering that the sum of the three line currents of the IM is zero, namely $i_a + i_b + i_c = 0$, currents in the (α, β) reference frame can be obtained from two line currents as follows:

$$\begin{bmatrix} i_\alpha \\ i_\beta \end{bmatrix} = \mathbf{T}\begin{bmatrix} i_a \\ i_b \\ -i_a - i_b \end{bmatrix}. \tag{13}$$

Departing from (12) and (13), the outputs from sensors can be represented in this reference frame as

$$\begin{aligned} i_{\alpha f} &= i_\alpha + m_\alpha \\ i_{\beta f} &= i_\beta + m_\beta \end{aligned} \tag{14}$$

where $m_\alpha = m_a$ and $m_\beta = \frac{1}{\sqrt{3}}m_a + \frac{2}{\sqrt{3}}m_b$. Thus, signals $i_{\alpha f}$ and $i_{\beta f}$ from (14) can be considered as the outputs of the system (9), represented in the (α, β) stationary reference frame. It is worth noting that m_α only depends on faults in sensor a while m_β depends on faults in both current sensors.

3.1.2. Faults in the $(\tilde{\alpha}, \tilde{\beta})$ reference frame

In a similar manner, currents in the $(\tilde{\alpha}, \tilde{\beta})$ reference frame can be obtained as:

$$\begin{bmatrix} i_{\tilde{\alpha}} \\ i_{\tilde{\beta}} \end{bmatrix} = \tilde{\mathbf{T}}\begin{bmatrix} i_a \\ i_b \\ -i_a - i_b \end{bmatrix}. \tag{15}$$

From (12) and (15), the outputs from sensors can be represented as

$$\begin{aligned} i_{\tilde{\alpha} f} &= i_{\tilde{\alpha}} + m_{\tilde{\alpha}} \\ i_{\tilde{\beta} f} &= i_{\tilde{\beta}} + m_{\tilde{\beta}} \end{aligned} \tag{16}$$

where $m_{\tilde{\alpha}} = m_b$ and $m_{\tilde{\beta}} = -\frac{1}{\sqrt{3}}m_b - \frac{2}{\sqrt{3}}m_a$. In this case, $m_{\tilde{\alpha}}$ depends on faults in sensor b while $m_{\tilde{\beta}}$ depends on faults in both current sensors.

Therefore, through the transformations (8) and (10) the IM model and the sensor faults can be represented in two stationary referent frames. In the following sections, the representation in the (α, β) frame is used to design a residual sensitive to the fault m_α, in order to isolate the faults in sensor a. Moreover, the representation in the $(\tilde{\alpha}, \tilde{\beta})$ frame is used to design a residual sensitive to the fault $m_{\tilde{\alpha}}$, in order to isolate the faults in sensor b.

3.2. Detectability and isolability of sensor faults

In this section, detectability and isolability of current sensor faults are studied with the geometric analysis. In order to apply the approach presented in Section 2, the IM model structure has to be similar to (1), where faults are represented as actuator faults (Espinoza-Trejo & Campos-Delgado, 2009). The most common methods to obtain this representation are applying a filter to the sensor signals (Alwi & Edwards, 2014) or an integrator (Zhang,

Swain, & Nguang, 2014). These methods increase the order of the system and its associated observers. Thus, the method used in the present work is based on Du, Jiang, and Shi (2014), where a transformation of states is used in order to obtain the required representation, without increasing the order of the system. With this approach, the transformation for model (9) is directly given by the output Eq. (14), replacing stator currents by $i_\alpha = i_{\alpha f} - m_\alpha$ and $i_\beta = i_{\beta f} - m_\beta$. As a result, the following representation is obtained:

$$\begin{aligned}
\dot{i}_{\alpha f} &= -a i_{\alpha f} + bc\lambda_\alpha + b\omega\lambda_\beta + du_\alpha + am_\alpha + \dot{m}_\alpha \\
\dot{i}_{\beta f} &= -a i_{\beta f} + bc\lambda_\beta - b\omega\lambda_\alpha + du_\beta + am_\beta + \dot{m}_\beta \\
\dot{\lambda}_\alpha &= L_M c i_{\alpha f} - c\lambda_\alpha - \omega\lambda_\beta - L_M c m_\alpha \\
\dot{\lambda}_\beta &= L_M c i_{\beta f} - c\lambda_\beta + \omega\lambda_\alpha - L_M c m_\beta \\
\dot{\omega} &= -kc_f\omega + kc_t(i_{\alpha f}\lambda_\beta - i_{\beta f}\lambda_\alpha) - kT_L + kc_t(\lambda_\alpha m_\beta - \lambda_\beta m_\alpha)
\end{aligned} \tag{17}$$

Note that it is straightforward to apply a similar transformation to model (11) in the $(\tilde{\alpha}, \tilde{\beta})$ reference frame, using the output Eq. (16).

In the following subsections, the FPRG solution is obtained for the IMD with three different objectives. The first one is to study the detectability of faults m_a and m_b when the load torque is considered an arbitrary input. The second objective is to study the isolability of the sensor fault m_a, while fault m_b is considered as a perturbation and the third one is to study the isolability of the sensor fault m_b. According to Section 2, three subsystems are obtained for the design of the FDIS. The studied cases are summarized in Table 2.

3.2.1. Detectability

Model (17) can be represented in a compact form as:

$$\begin{aligned}
\dot{\mathbf{x}} &= \mathbf{g}(\mathbf{x}) + \mathbf{B}_0\mathbf{u} + \mathbf{L}_0\mathbf{f} + \mathbf{D}_0 w \\
\mathbf{y} &= \mathbf{C}_0\mathbf{x}
\end{aligned} \tag{18}$$

where $\mathbf{x} = [x_1, x_2, x_3, x_4, x_5]^\top = [i_{\alpha f}, i_{\beta f}, \lambda_\alpha, \lambda_\beta, \omega]^\top$ is the state vector, $\mathbf{y} = [\mathbf{y}_1, \mathbf{y}_2, \mathbf{y}_3]^\top$ is the output vector, $\mathbf{u} = [u_\alpha, u_\beta]^\top$ is the known input vector, $\mathbf{f} = [m_\alpha, \dot{m}_\alpha, m_\beta, \dot{m}_\beta]^\top$ is the fault vector, $w = T_L - c_t(x_3 m_\beta - x_4 m_\alpha)$ is the perturbation and:

$$\mathbf{g}(\mathbf{x}) = \begin{bmatrix} -ax_1 + bcx_3 + bx_5x_4 \\ -ax_2 + bcx_4 - bx_5x_3 \\ L_M c x_1 - cx_3 - x_5x_4 \\ L_M c x_2 - cx_4 + x_5x_3 \\ -kc_f x_5 + kc_t(x_1x_4 - x_2x_3) \end{bmatrix},$$

$$\mathbf{B}_0 = \begin{bmatrix} d & 0 \\ 0 & d \\ 0 & 0 \\ 0 & 0 \\ 0 & 0 \end{bmatrix}, \quad \mathbf{C}_0 = \begin{bmatrix} 1 & 0 & 0 & 0 & 0 \\ 0 & 1 & 0 & 0 & 0 \\ 0 & 0 & 0 & 0 & 1 \end{bmatrix},$$

$$\mathbf{L}_0 = \begin{bmatrix} a & 1 & 0 & 0 \\ 0 & 0 & a & 1 \\ -L_M c & 0 & 0 & 0 \\ 0 & 0 & -L_M c & 0 \\ 0 & 0 & 0 & 0 \end{bmatrix}, \quad \mathbf{D}_0 = \begin{bmatrix} 0 \\ 0 \\ 0 \\ -k \end{bmatrix}. \tag{19}$$

Table 2
Studied cases of sensor faults.

Objective	Detectability	Isolation of m_a	Isolation of m_b
Faults	m_a, m_b	m_a	m_b
Perturbations	T_L	m_b, T_L	m_a, T_L

Using (18), as described in Section 2, the algorithms presented in De Persis and Isidori (2001) can be computed to obtain the following observability codistribution:

$$\boldsymbol{\Omega} = \text{span}\{[dx_1, dx_2, dx_3, dx_4]\}. \tag{20}$$

A change of coordinates of the output space is given by the transformation described in (5), with

$$\mathbf{H}_1 = \begin{bmatrix} 1 & 0 & 0 \\ 0 & 1 & 0 \end{bmatrix}, \quad \mathbf{H}_2 = [0 \;\; 0 \;\; 1]$$

and using $\boldsymbol{\psi}_1 \triangleq [\psi_{11}, \psi_{12}]^\top$ and $\boldsymbol{\psi}_2 \triangleq [\psi_{21}]$. Moreover, a transformation of state space is given by (7), where

$$\boldsymbol{\Phi}_1 = \begin{bmatrix} 1 & 0 & 0 & 0 & 0 \\ 0 & 1 & 0 & 0 & 0 \\ 0 & 0 & 1 & 0 & 0 \\ 0 & 0 & 0 & 1 & 0 \end{bmatrix}, \quad \mathbf{H}_2\mathbf{C}_0 = [0 \;\; 0 \;\; 0 \;\; 0 \;\; 1]$$

and states are $\mathbf{z}_1 \triangleq [z_{11}, z_{12}, z_{13}, z_{14}]^\top$ and $\mathbf{z}_2 \triangleq [z_{21}]$. Applying these transformations, the following subsystem is obtained:

$$\begin{aligned}
\dot{z}_{11} &= -az_{11} + bcz_{13} + bz_{14}\psi_{21} + du_1 + am_\alpha + \dot{m}_\alpha \\
\dot{z}_{12} &= -az_{12} + bcz_{14} - bz_{13}\psi_{21} + du_2 + am_\beta + \dot{m}_\beta \\
\dot{z}_{13} &= L_M c z_{11} - cz_{13} - z_{14}\psi_{21} - L_M c m_\alpha \\
\dot{z}_{14} &= L_M c z_{12} - cz_{14} + z_{13}\psi_{21} - L_M c m_\beta \\
\psi_{11} &= z_{11} \\
\psi_{12} &= z_{12}.
\end{aligned} \tag{21}$$

Note that, in the obtained subsystem, the angular speed $\omega = \psi_{21}$ is now considered as a known input. The output of this subsystem is decoupled from the load torque but sensitive to both sensor faults, namely m_a and m_b. Residuals for fault detection could be designed by using an observer based on subsystem (21). These residuals will be sensitive to faults in both sensors, but additional processing and considerations are needed in order to accomplish the isolation (Najafabadi et al., 2011).

The condition that the speed sensor is required was obtained because an arbitrary load torque was assumed. This condition could be avoided if more relaxed specifications for fault isolation or the load torque are considered, such as a constant torque. A speed estimator could be implemented in order to provide the speed signal required by the FDIS. Nevertheless, in general, speed estimators requires the current measurements. Thus, if a current sensor fault occurs, the speed estimation will be affected. This degraded speed signal will increase residual levels in both observers, interfering with the isolation of the fault.

3.2.2. Isolation of faults in sensor a

In order to isolate faults in sensor a, a subsystem insensitive to faults in sensor b and load torque must be obtained. With this end, $w_\beta \triangleq \dot{m}_\beta$ and $x_6^a \triangleq m_\beta$ are defined, where the last one is considered as a new state of (17). Then, from (9), IM model in the (α, β) reference frame can be represented as:

$$\begin{aligned}
\dot{\mathbf{x}}^a &= \mathbf{g}^a(\mathbf{x}^a) + \mathbf{B}\mathbf{u}^a + \mathbf{L}(\mathbf{x}^a)\mathbf{f}^a + \mathbf{D}\mathbf{w}^a \\
\mathbf{y}^a &= \mathbf{C}\mathbf{x}^a
\end{aligned} \tag{22}$$

where $\mathbf{x}^a = [x_1^a, x_2^a, x_3^a, x_4^a, x_5^a, x_6^a]^\top = [i_{\alpha f}, i_{\beta f}, \lambda_\alpha, \lambda_\beta, \omega, m_\beta]^\top$ is the state vector, $\mathbf{u}^a = [u_1^a, u_2^a]^\top = [u_\alpha, u_\beta]^\top$ is the known input vector, $\mathbf{f}^a = [m_\alpha, \dot{m}_\alpha]^\top$ is the fault vector, $\mathbf{w}^a = [T_L - c_t x_3^a m_\beta, w_\beta]^\top$ is the perturbation vector and:

$$\mathbf{g}^a(\mathbf{x}^a)=\begin{bmatrix} -ax_1^a+bcx_3^a+bx_5^ax_4^a \\ -ax_2^a+bcx_4^a-bx_5^ax_3^a \\ L_Mcx_1^a-cx_3^a-x_5^ax_4^a \\ L_Mcx_2^a-cx_4^a+x_5^ax_3^a \\ -kc_fx_5^a+kc_t(x_1^ax_4^a-x_2^ax_3^a)-kc_t(x_3^ax_6^a) \\ 0 \end{bmatrix},$$

$$\mathbf{B}=\begin{bmatrix} d & 0 \\ 0 & d \\ 0 & 0 \\ 0 & 0 \\ 0 & 0 \\ 0 & 0 \end{bmatrix},\quad \mathbf{C}=\begin{bmatrix} 1 & 0 & 0 & 0 & 0 & 0 \\ 0 & 1 & 0 & 0 & 0 & 0 \\ 0 & 0 & 0 & 0 & 1 & 0 \end{bmatrix},$$

$$\mathbf{D}=\begin{bmatrix} 0 & 0 \\ 0 & 0 \\ 0 & 0 \\ 0 & 0 \\ 1 & 0 \\ 0 & 1 \end{bmatrix},\quad \mathbf{L}(\mathbf{x}^a)=\begin{bmatrix} a & 1 \\ 0 & 0 \\ -L_Mc & 0 \\ 0 & 0 \\ kc_tx_4^a & 0 \\ 0 & 0 \end{bmatrix}. \tag{23}$$

By using algorithms described in Section 2, the following observability codistribution can be obtained:

$$\mathbf{\Omega}^a=\text{span}\left\{\begin{bmatrix} 1 & 0 & 0 & 0 & 0 & 0 \\ 0 & 0 & 1 & 0 & 0 & 0 \\ 0 & 0 & 0 & 1 & 0 & 0 \\ 0 & 1 & 0 & 0 & 0 & -1 \end{bmatrix}\right\}. \tag{24}$$

In order to obtain the subsystem, a change of coordinates of the output space is obtained by the transformation $\left[\psi_1^a,\ \psi_2^a\right]^\top=\tilde{\mathbf{H}}\mathbf{y}^a$, where

$$\tilde{\mathbf{H}}\triangleq\begin{bmatrix}\tilde{\mathbf{H}}_1\\ \tilde{\mathbf{H}}_2\end{bmatrix}, \tag{25}$$

$$\tilde{\mathbf{H}}_1=[1\ \ 0\ \ 0],\quad \tilde{\mathbf{H}}_2=\begin{bmatrix}0 & 0 & 1\\ 0 & 1 & 0\end{bmatrix}. \tag{26}$$

The outputs in the new coordinates are $\boldsymbol{\psi}_1^a\triangleq[\psi_{11}^a]$ and $\boldsymbol{\psi}_2^a\triangleq[\psi_{21}^a,\ \psi_{22}^a]$. Moreover, transformation of state space is obtained by $[z_1^a,\ z_2^a]^\top=\tilde{\mathbf{\Phi}}\mathbf{x}^a$, where

$$\tilde{\mathbf{\Phi}}\triangleq\begin{bmatrix}\tilde{\mathbf{\Phi}}_1\\ \tilde{\mathbf{H}}_2\mathbf{C}\end{bmatrix},\quad \tilde{\mathbf{\Phi}}_1=\begin{bmatrix}1 & 0 & 0 & 0 & 0 & 0\\ 0 & 0 & 1 & 0 & 0 & 0\\ 0 & 0 & 0 & 1 & 0 & 0\\ 0 & 1 & 0 & 0 & 0 & -1\end{bmatrix}. \tag{27}$$

States in the new coordinates are $\mathbf{z}_1^a\triangleq[z_{11}^a,\ z_{12}^a,\ z_{13}^a,\ z_{14}^a]^\top$ and $\mathbf{z}_2^a\triangleq[z_{21}^a,\ z_{22}^a]^\top$. Applying these transformations, the subsystem can be described as:

$$\begin{aligned}\dot{\xi}_1^a&=-a\xi_1^a+f_1(\boldsymbol{\xi}_2^a,\psi_{21}^a)+du_1^a+am_\alpha+\dot{m}_\alpha\\ \dot{\boldsymbol{\xi}}_2^a&=\boldsymbol{f}_2(\xi_1^a,\boldsymbol{\xi}_2^a,u_2^a,\psi_{21}^a)+\boldsymbol{\zeta}(m_\alpha)\\ \psi_{11}^a&=\xi_1^a\end{aligned} \tag{28}$$

where $\xi_1^a=z_{11}^a$, $\boldsymbol{\xi}_2^a=[\xi_{21}^a,\ \xi_{22}^a,\ \xi_{23}^a]^\top=[z_{12}^a,\ z_{13}^a,\ z_{14}^a]^\top$ and

$$f_1(\boldsymbol{\xi}_2^a,\psi_{21}^a)=bc\xi_{21}^a+b\xi_{22}^a\psi_{21}^a,$$

$$\boldsymbol{f}_2(\xi_1^a,\boldsymbol{\xi}_2^a,u_2^a,\psi_{21}^a)=\begin{bmatrix}L_Mc\xi_1^a-c\xi_{21}^a-\xi_{22}^a\psi_{21}^a\\ L_Mc\xi_{23}^a-c\xi_{22}^a+\xi_{21}^a\psi_{21}^a\\ -a\xi_{23}^a+bc\xi_{22}^a-b\xi_{21}^a\psi_{21}^a+du_2^a\end{bmatrix},$$

$$\boldsymbol{\zeta}(m_\alpha)=\begin{bmatrix}-L_Mcm_\alpha\\ 0\\ 0\end{bmatrix}. \tag{29}$$

Thus, the output of subsystem (28) is sensitive to the sensor a fault signal, namely $m_a=m_\alpha$, and its first derivative $\dot{m}_\alpha$. As can be observed from (28) and (14), the subsystem is decoupled from signal m_β, which depends on the fault in sensor b, namely m_b. This subsystem is useful for the design of an observer-based residual generator. The output residual will be sensitive to faults in sensor a but insensitive to faults in sensor b and load torque changes. Finally, it is worth noting that the observer will use the rotor speed signal $\omega=\psi_{21}^a$ as an input.

3.2.3. Isolation of faults in sensor b

The same procedure is followed to study the isolation of faults in sensor b. In this case, the IM model in the $(\tilde{\alpha},\tilde{\beta})$ reference frame (11) is used in order to represent the system in the compact form:

$$\begin{aligned}\dot{\mathbf{x}}^b&=\mathbf{g}^b(\mathbf{x}^b)+\mathbf{B}\mathbf{u}^b+\mathbf{L}(\mathbf{x}^b)\mathbf{f}^b+\mathbf{D}\mathbf{w}^b\\ \mathbf{y}^b&=\mathbf{C}\mathbf{x}^b\end{aligned} \tag{30}$$

where $\mathbf{B}$, $\mathbf{C}$ and $\mathbf{D}$ are defined as in the previous case, and

$$\mathbf{x}^b=\left[x_1^b,\ x_2^b,\ x_3^b,\ x_4^b,\ x_5^b,\ x_6^b\right]^\top=\left[i_{\tilde{\alpha}f},\ i_{\tilde{\beta}f},\ \lambda_{\tilde{\alpha}},\ \lambda_{\tilde{\beta}},\ \omega,\ m_{\tilde{\beta}}\right]^\top,$$

$$\mathbf{u}^b=\left[u_1^b,\ u_2^b\right]^\top=\left[u_{\tilde{\alpha}},\ u_{\tilde{\beta}}\right]^\top,$$

$$\mathbf{f}^b=\left[m_{\tilde{\alpha}},\ \dot{m}_{\tilde{\alpha}}\right]^\top,$$

$$\mathbf{w}^b=\left[T_L-c_tx_3^bm_{\tilde{\beta}},\ w_{\tilde{\beta}}\right]^\top,$$

$$\mathbf{g}^b(\mathbf{x}^b)=\begin{bmatrix} -ax_1^b+bcx_3^b+bx_5^bx_4^b\\ -ax_2^b+bcx_4^b-bx_5^bx_3^b\\ L_Mcx_1^b-cx_3^b-x_5^bx_4^b\\ L_Mcx_2^b-cx_4^b+x_5^bx_3^b\\ -kc_fx_5^b+kc_t(x_1^bx_4^b-x_2^bx_3^b)-kc_t(x_3^bx_6^b)\\ 0\end{bmatrix},$$

$$\mathbf{L}(\mathbf{x}^b)=\begin{bmatrix} a & 1\\ 0 & 0\\ -L_Mc & 0\\ 0 & 0\\ kc_tx_4^b & 0\\ 0 & 0\end{bmatrix}. \tag{31}$$

The outputs for model (30) in the new coordinates are obtained by $\left[\psi_1^b,\ \psi_2^b\right]^\top=\tilde{\mathbf{H}}\mathbf{y}^b$, whereas state space is obtained by $\left[z_1^b,\ z_2^b\right]^\top=\tilde{\mathbf{\Phi}}\mathbf{x}^b$, where $\mathbf{z}_1^b\triangleq\left[z_{11}^b,\ z_{12}^b,\ z_{13}^b,\ z_{14}^b\right]^\top$, $\mathbf{z}_2^b\triangleq\left[z_{21}^b,\ z_{22}^b\right]^\top$ $\boldsymbol{\psi}_1^b\triangleq[\psi_{11}^b]$ and $\boldsymbol{\psi}_2^b\triangleq\left[\psi_{21}^b,\ \psi_{22}^b\right]^\top$. The resulting subsystem can be described as:

$$\begin{aligned}\dot{\xi}_1^b&=-a\xi_1^b+f_1(\boldsymbol{\xi}_2^b,\psi_{21}^b)+du_1^b+am_{\tilde{\alpha}}+\dot{m}_{\tilde{\alpha}}\\ \dot{\boldsymbol{\xi}}_2^b&=\boldsymbol{f}_2(\xi_1^b,\boldsymbol{\xi}_2^b,u_2^b,\psi_{21}^b)+\boldsymbol{\zeta}(m_{\tilde{\alpha}})\\ \psi_{11}^b&=\xi_1^b\end{aligned} \tag{32}$$

where $\xi_1^b=z_{11}$, $\boldsymbol{\xi}_2^b=\left[\xi_{21}^b,\ \xi_{22}^b,\ \xi_{23}^b\right]^\top=\left[z_{12}^b,\ z_{13}^b,\ z_{14}^b\right]^\top$ and

$$f_1(\xi_2^b, \psi_{21}^b) = bc\xi_{21}^b + b\xi_{22}^b\psi_{21}^b,$$
$$\boldsymbol{f}_2(\xi_1^b, \boldsymbol{\xi}_2^b, u_2^b, \psi_{21}^b) = \begin{bmatrix} L_M c\xi_1^b - c\xi_{21}^b - \xi_{22}^b\psi_{21}^b \\ L_M c\xi_{23}^b - c\xi_{22}^b + \xi_{21}^b\psi_{21}^b \\ -a\xi_{23}^b + bc\xi_{22}^b - b\xi_{21}^b\psi_{21}^b + du_2^b \end{bmatrix}$$
$$\zeta(m_{\tilde{a}}) = \begin{bmatrix} -L_M c m_{\tilde{a}} \\ 0 \\ 0 \end{bmatrix}. \tag{33}$$

In this case, the output of subsystem (32) is sensitive to the fault in sensor b, namely $m_b = m_{\tilde{a}}$, and its first derivative $\dot{m}_{\tilde{a}}$. Also, as can be observed from (32) and (16), the subsystem is decoupled from signal $m_{\tilde{\beta}}$, which depends on the fault in sensor a, namely m_a. Subsystems (28) and (32) can be used for the design of decoupled residual signals for the FDIS shown in Fig. 1, as presented in the following section.

3.3. Design of the bank of observers

As an example, observers for residual generation are designed in this section, based on subsystems (28) and (32). The proposed observers are designed from a combination of sliding mode observers (SMO) and high gain observers (HGO). In last years, SMO have been successfully used for FDIS in critical applications such as aerospace. They have proven to be an effective way to generate residuals to detect and even reconstruct system faults, including sensor faults (Alwi & Edwards, 2014; Rahme & Meskin, 2015). HGO are well-known techniques for fast and reliable state estimation, which have been proposed for several classes of nonlinear systems (Busawon & De Leon-Morales, 2000). In present paper, the SMO is used to generate residuals based on the equivalent output error injection term while the HGO is designed to estimate the subsystems states after the sliding surface is reached.

Observers are described using the same set of equations denoted by $\boldsymbol{\Sigma}^i$, where $i \in \{a, b\}$ refers to the observer for subsystem (28) and (32), respectively, as:

$$\boldsymbol{\Sigma}^i \begin{cases} \dot{\hat{\xi}}_1^i = -a\hat{\xi}_1^i + f_1(\hat{\boldsymbol{\xi}}_2^i, \psi_{21}^i) + du_1^i - bc\nu_i \\ \dot{\hat{\boldsymbol{\xi}}}_2^i = \boldsymbol{f}_2(\xi_1^i, \hat{\boldsymbol{\xi}}_2^i, u_2^i, \psi_{21}^i) - \boldsymbol{\Gamma}(\psi_{21}^i)\nu_i \\ \hat{\psi}_{11}^i = \hat{\xi}_1^i \end{cases} \tag{34}$$

where $\hat{\xi}_1^i$ and $\hat{\boldsymbol{\xi}}_2^i = \left[\hat{\xi}_{21}^i, \hat{\xi}_{22}^i, \hat{\xi}_{23}^i\right]^\top$ are estimated states, $\psi_{21}^i = \omega$ is the angular speed, $\boldsymbol{\Gamma}(\psi_{21}^i)$ is a feedback gain which will be designed in next section, and

$$f_1(\hat{\boldsymbol{\xi}}_2^i, \psi_{21}^i) = bc\hat{\xi}_{21}^i + b\hat{\xi}_{22}^i\psi_{21}^i,$$
$$\boldsymbol{f}_2(\xi_1^i, \hat{\boldsymbol{\xi}}_2^i, u_2^i, \psi_{21}^i) = \begin{bmatrix} L_M c\xi_1^i - c\hat{\xi}_{21}^i - \hat{\xi}_{22}^i\psi_{21}^i \\ L_M c\hat{\xi}_{23}^i - c\hat{\xi}_{22}^i + \hat{\xi}_{21}^i\psi_{21}^i \\ -a\hat{\xi}_{23}^i + bc\hat{\xi}_{22}^i - b\hat{\xi}_{21}^i\psi_{21}^i + du_2^i \end{bmatrix}. \tag{35}$$

Signals ν_i represent the discontinuous functions of the SMO. For its implementation, the following continuous approximation is used (Alwi & Edwards, 2014):

$$\nu_i = k_\nu \operatorname{sign}(\hat{\xi}_1^i - \xi_1^i) \approx k_\nu \frac{e_1^i}{\left|e_1^i\right| + \delta} \tag{36}$$

where $e_1^i = \hat{\xi}_1^i - \xi_1^i$ are the estimation errors of ξ_1^i, k_ν is a positive gain and δ is a positive scalar.

Fig. 3 shows a diagram with the observers structure, where u_a, u_b, u_c and ω are inputs taken from the IMD. Outputs ν_i are the residual signals. The observers estimation error and the behavior of the residuals is described below.

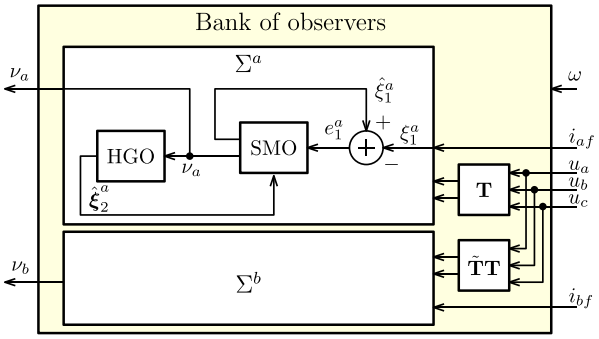

Fig. 3. Proposed bank of observers structure.

3.3.1. Residual signals without faults

First, it is assumed that there are no sensor faults, i.e. $m_i = \dot{m}_i = 0$. In this condition, the dynamics of the estimation errors $e_1{}^i$ are

$$\dot{e}_1^i = -ae_1^i + f_1(\boldsymbol{e}_2^i, \psi_{21}^i) - bc\nu_i \tag{37}$$

where $\boldsymbol{e}_2^i = \left[e_{21}^i, e_{22}^i, e_{23}^i\right]^\top = \hat{\boldsymbol{\xi}}_2^i - \boldsymbol{\xi}_2^i$ are the estimation errors of $\boldsymbol{\xi}_2^i$. By considering the Lyapunov function $V_1^i = \frac{1}{2}\left(e_1^i\right)^2$ and assuming that $\nu_i \approx k_\nu \operatorname{sign}(e_1^i)$, the following result can be obtained:

$$\begin{aligned} \dot{V}_1^i &= \dot{e}_1^i e_1^i \\ &= -a\left(e_1^i\right)^2 + f_1(\boldsymbol{e}_2^i, \psi_{21}^i)e_1^i - bck_\nu \operatorname{sign}(e_1^i)e_1^i \\ &= -bck_\nu\left|e_1^i\right| - a\left(e_1^i\right)^2 + f_1(\boldsymbol{e}_2^i, \psi_{21}^i)e_1^i \end{aligned} \tag{38}$$

with $bc > 0$. Therefore, if gain k_ν is chosen high enough such that $k_\nu > \frac{1}{bc}\max\left(\left|f_1\left(\boldsymbol{e}_2^i, \psi_{21}^i\right)e_1^i\right|\right)$, then $\dot{V}_1 < 0$ until the sliding surface $e_1^i = 0$ is reached, which guarantees that the estimation error e_1^i converges to zero. When this condition is satisfied, and taking into account (28), (32) and (34), the following expression can be obtained:

$$\nu_{i\_eq} = \frac{1}{bc}f_1(\boldsymbol{e}_2^i, \psi_{21}^i) = e_{21}^i + \frac{1}{c}\psi_{21}^i e_{22}^i \tag{39}$$

where ν_{i_eq} is the equivalent output error injection.

Once the sliding surface $e_1^i = 0$ is reached, the dynamics of the estimation errors $\boldsymbol{e}_2^i$ are given by

$$\dot{\boldsymbol{e}}_2^i = \boldsymbol{f}_{2\nu}(\boldsymbol{e}_2^i, \psi_{21}^i) - \boldsymbol{\Gamma}(\psi_{21}^i)\nu_{i\_eq} \tag{40}$$

where

$$\boldsymbol{f}_{2\nu}(\boldsymbol{e}_2^i, \psi_{21}^i) = \begin{bmatrix} -ce_{21}^i - e_{22}^i\psi_{21}^i \\ e_{21}^i\psi_{21}^i - ce_{22}^i + L_M ce_{23}^i \\ -b\,e_{21}^i\psi_{21}^i + bce_{22}^i - ae_{23}^i \end{bmatrix} \tag{41}$$

By analyzing (40), it is noted that the structure of this error dynamics is similar to the class of nonlinear single-output systems threated in Busawon and De Leon-Morales (2000). Therefore, it is straightforward to apply the HGO design method proposed in previously cited paper. Following this design method, the feedback gain $\boldsymbol{\Gamma}(\psi_{21}^i)$ has the form:

$$\mathbf{\Gamma}(\psi_{21}^i) = \mathbf{M}^{-1}(\psi_{21}^i)[\mathbf{L}\left(\psi_{21}^i\right) + \mathbf{\Theta K}] \tag{42}$$

where

$$\mathbf{M}(\psi_{21}^i) = \begin{bmatrix} bc & 0 & 0 \\ bc^2 + abc & -bc\psi_{21}^i & 0 \\ -abc^2 - L_M b^2 c^2 & -abc\psi_{21}^i & -L_M bc^2\psi_{21}^i \end{bmatrix}$$

$$\mathbf{L}(\psi_{21}^i) = \begin{bmatrix} -a - 2c \\ L_M bc^2 - c^2 - 2ac - \left(\psi_{21}^i\right)^2 \\ L_M bc^3 - ac^2 + (L_M bc - a)\left(\psi_{21}^i\right)^2 \end{bmatrix}$$

$$\mathbf{K} = \begin{bmatrix} k_1 \\ k_2 \\ k_3 \end{bmatrix}, \quad \mathbf{\Theta} = \begin{bmatrix} \theta & 0 & 0 \\ 0 & \theta^2 & 0 \\ 0 & 0 & \theta^3 \end{bmatrix}. \tag{43}$$

The assumption that the IM is working at a speed different from zero, namely $|\omega| > 0$, was required in order to apply the procedure of Busawon and De Leon-Morales (2000). Additionally, gain $\mathbf{K}$ must be selected in order that the following matrix

$$\mathbf{R} \triangleq \begin{bmatrix} 0 & 1 & 0 \\ 0 & 0 & 1 \\ 0 & 0 & 0 \end{bmatrix} + \mathbf{K}[1 \;\; 0 \;\; 0] \tag{44}$$

has all its eigenvalues with negative real part. If above conditions are satisfied, there exists $\theta_0 > 0$ such that for all $\theta > \theta_0$, estimation errors $\mathbf{e}_2^i$ will tend exponentially to zero. Thus, considering fault signals $m_i = \dot{m}_i = 0$, after the sliding surface $e_1^i = 0$ is reached signals ν_i will tend to zero, as can be deduced from (39). The convergence of the estimation errors is validated by simulation results in Appendix A.

3.3.2. Residual signals considering faults

Now, fault signals $m_i \neq 0$ are considered, assuming that m_i and $\dot{m}_i$ are bounded. Under this assumption, a large enough value of k_ν, such that $k_\nu > \frac{1}{bc}\max\left(\left| f_1\left(\mathbf{e}_2^i, \psi_{21}^i\right)e_1^i + \frac{a}{bc}m_i e_1^i + \frac{1}{bc}\dot{m}_i e_1^i \right|\right)$, still guarantees that the sliding surface $e_1^i = 0$ is reached. In this case, from (28), (32) and (34) the following expression can be obtained

$$\nu_{i\_eq} = \frac{1}{bc}f_1(\mathbf{e}_2^i, \psi_{21}^i) + \frac{a}{bc}m_i + \frac{1}{bc}\dot{m}_i. \tag{45}$$

Therefore, the equivalent output error injection will be affected by the fault and its derivative, and by the dynamics of $f_1(\mathbf{e}_2^i, \psi_{21}^i)$ which depend on the estimation error $\mathbf{e}_2^i$.

Based on the obtained results, the following conclusions can be enumerated:

1. Residual signals ν_i tend to zero if sensors are healthy.
2. Under a current sensor fault, the corresponding residual will have a non-zero value that depends on the fault m_i, as obtained in (45).
3. Signals ν_i are very sensitive to abrupt faults because of its dependence on the fault signal derivatives $\dot{m}_i$.
4. Each residual ν_i is affected only by faults in the sensor i, as it was concluded in Section 3.2.

An additional potential application of the observers is the estimation of IM currents using only one line current sensor. This can be noted from the transformation (27), where the equality $\xi_{23}^a = i_\beta$ can be obtained. Thus, signal $\hat{\xi}_{23}^a$ could be used as an estimate of current i_β. Then, from the (α, β) transformation defined in (8), line currents can be reconstructed using the observer $\mathbf{\Sigma}^a$ in the case that a fault is detected in sensor b. In a similar manner, $\mathbf{\Sigma}^b$ can be used to estimate the line currents if a fault occurs in sensor a. These estimates may be useful to implement FTD based on virtual sensors (Raisemche et al., 2014).

It must be noted that, the same as other model-based strategies, the proposed FDIS design strategy needs a preliminary knowledge of the IM parameters. However, in any closed loop IM drive, motor parameters are needed for a correct tuning of the closed-loop controller. Therefore, such parameters are usually obtained at a self-commissioning stage (Espinoza-Trejo & Campos-Delgado, 2009). Nonetheless, state estimation errors and unmodelled non-linearities can affect the residuals signals. Thus, if the effect of uncertainties in models (28) and (32) is important, robust techniques must be investigated for synthesizing the observers for residual generation (Zhang et al., 2014).

3.4. Post-processing of the residuals signals

As it was shown in Fig. 1, fault detection and isolation are carried out by the post-processing of the residuals ν_i generated by the bank of observers. In this work, the post-processing stage consists on the estimation of residuals peak values. The estimation is done by an envelope detector filter, composed by a fall-rate limiter that is fed by the absolute value of signals ν_i (Bisheimer, De Angelo, Solsona, & Garcia, 2008). Then, estimated peak values are compared with a constant threshold C_{th}. After residuals post-processing, the FDIS produces two logic signals F_a and F_b which indicate the detection of a fault in sensor a or sensor b, respectively.

Note that although from the theoretical analysis residuals are sensitive to any non-zero fault signal m_i, from the practical point of view the minimum fault level that can be diagnosed depends on different aspects, such as: sensor characteristics, model uncertainties, A/D converter resolution, numerical precision of the microcontroller, noise level, among others. Moreover, it also depends on the threshold level used for the residual evaluation. This threshold is usually set after some measurements under normal operating conditions, according to measurement noise level and disturbances, in order to avoid false alarms (Zhang et al., 2013).

In order to establish the threshold level, in this work different tests were performed on the experimental setup. The maximum noise level of the residual signals under healthy sensor condition was measured. Then, threshold C_{th} was set as twice the measured maximum noise. The selected threshold level is shown in Table 3.

4. Results

Here, the experimental setup used to validate the FDIS designed in Section 3 is presented together with experimental results. In addition, simulation results of residuals response against parameter variations and load changes are analyzed.

4.1. Experimental setup

Fig. 4 shows the block diagram of the experimental setup used to validate the proposed FDIS. The system described in Section 3 was implemented in a PC using a fixed step-size Bogacki–Shampine solver from MATLAB environment, with the parameters listed in Table 3. Although the strategy was programmed on a PC, it has a low computational requirement. For this reason, it can be easily implemented in the microcontroller of a variable speed drive.

The FDIS was tested using a low voltage 0.75 kW squirrel cage IM, whose rated variables and parameters are provided in Table 3. With the objective of validating the method with the IM under load, a second standard 5.5 kW IM with torque control was used as load.

Table 3
IM and FDIS parameters.

IM			
Power	0.75 kW	Frequency	50 Hz
Line voltage	26.4 V	Rated speed	1435 RPM
R_s	69.7 mΩ	R_r	347.1 mΩ
L_s, L_r	0.11 mH	L_M	2.66 mH
P	2	J	0.00294 kgm^2
Current sensors: LEM LA 125-P			
Primary nominal current rms		125 A	
Frequency bandwidth (−1 dB)		0–100 kHz	
Accuracy		±0.6%	
FDIS			
k_ν	10	θ	5
k_1	30	k_2	400
k_3	2000	δ	1
C_{th}	0.05		

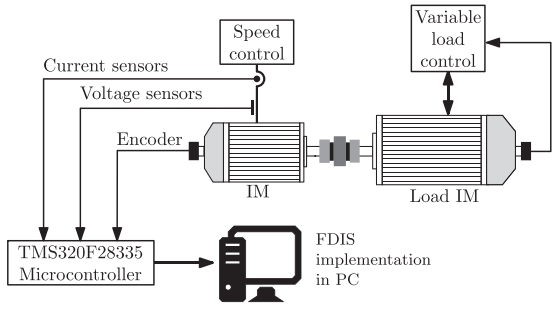

Fig. 4. Experimental setup.

An open-loop speed control was used during the experimental tests. This control was selected in order to avoid negative effects caused by sensor faults when IMD use closed-loop speed control, such as over currents (Aguilera et al., 2012). In case of closed-loop control is used, a FTD is needed to avoid those negative effects (Shi & Krishnamurthy, 2014). Nevertheless, FTD is not the aim of this paper and only the FDIS is validated.

Variables required by the FDIS were measured using two hall-effect current sensors, two voltage sensors and a digital encoder. The measured signals were acquired using a TMS320F28335 microcontroller, with a sample period $T_s = 1$ ms. Details about current sensors are shown in Table 3. With the experimental setup described above, the results shown in the following sub-section were obtained.

4.2. Experimental results

With the IM working at constant speed and without faults, a sudden load torque variation from 50% to 90% of the rated load torque at $t = 0.93$ s is applied. The torque variation causes a deceleration of the rotor and an increase of the line currents, see Fig. 5(a). Under this condition, residuals are not affected, as it is shown in Fig. 5(b).

At $t = 1.2$ s disconnection fault of sensor a occurs, this means that the signal provided by the sensor is made zero, see Fig. 5(a). The fault is generated into the implemented software by introducing a fault signal $m_a = -i_a$, where m_a is defined in (12). After this fault, the value of $|\nu_a|$ increases over the threshold level, which is reported by changing the signal F_a from '0' to '1' at $t = 1.201$ s, see Fig. 5(c). It is worth noting that the fault detection time corresponds to one sample period, namely 1 ms, which is faster than previously reported results.

As it was demonstrated by (45), residuals depend on the fault signals m_i and its derivatives $\dot{m}_i$. This fact causes a significant

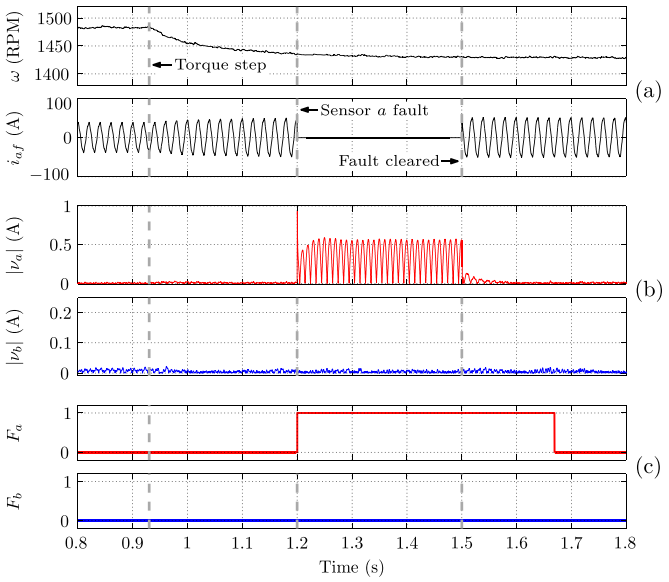

Fig. 5. Experimental results during a single fault in sensor a and load change. (a) Measured speed and line a current, (b) residuals and, (c) diagnostic signals.

transient in the absolute value of ν_a at $t = 1.2$ s. This feature shows that residuals are highly sensitive to sudden sensor faults improving in this way the fault detection time.

Fault detection time is a key topic for the design of a FTD, as it was stated in Section 1. For instance, in electric traction applications, a detection time below 5 ms is at least required in order to avoid negative effects over the IMD, as it was reported in Aguilera et al. (2012). Thus, the FDIS proposed in the present paper could be used in such applications.

From a practical point of view, the dependence on the fault derivative can produce an increase of residual levels under normal condition if high frequency noise is present in the measurements. Thus, the signals from the sensors must be passed trough a low-pass filter after being used by the FDIS. The cutoff frequency of this filter has to be selected to balance the trade-off between sensitivity to the fault derivative and noise level reduction.

The fault in sensor a is removed at $t = 1.5$ s and the fault detection signal F_a changes from '1' to '0' at $t = 1.69$ s, reporting that the sensor is again operating normally. This is an important feature in order to recover the system after a short duration fault. Note that along this experiment, signal ν_b is not affected by the fault in sensor a, demonstrating that residuals are decoupled from each other.

Fig. 6 shows the behavior of the FDIS during multiple sensor faults. Offset and gain faults were selected in order to analyze the FDIS performance. These faults are very common in practical applications, nevertheless they are not generally treated in the literature. They could be caused, for example, by a sudden or gradual detuning of sensors as a consequence its aging process. At $t = 2.2$ s a sudden offset fault occurs in sensor b, with an offset level of 30% of the rated IM line current, see Fig. 6(a). In the present paper, this fault is generated by introducing a sudden fault signal $m_a = f_0$, with f_0 constant. This fault causes an increase of $|\nu_b|$ and the change of signal F_b from '0' to '1', as it is shown in Fig. 6(b) and (c). The fault detection time is also of one sample period for this fault. Note that signal ν_a is not affected by the fault in sensor b.

With the offset fault present in sensor b, a progressive gain reduction fault occurs in sensor a at $t = 2.7$ s. The fault is generated by introducing a fault signal $m_a = -k_{fg} i_a$, where the scalar k_{fg} varies linearly from 0 to 0.55 in $2.7\text{ s} < t < 3$ s, see Fig. 6(a). This fault produces a progressive rise of residual $|\nu_a|$, see Fig. 6(b). Note that for any progressive faults, detection time depends on the fault evolution and the threshold level. In this case, the residual

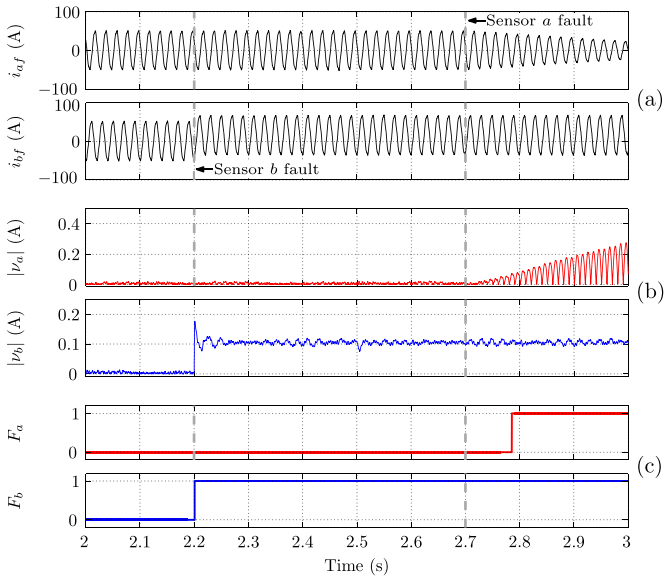

Fig. 6. Experimental results during multiple sensor faults. (a) Measured currents, (b) residuals and, (c) diagnostic signals.

increases above the threshold level at $t = 2.79$ s, where the fault produces a reduction of 18% in measured current. Once the residual reaches the selected threshold, the fault is detected in one sample period. When the gain fault is reported, both fault indicators F_a and F_b are active, demonstrating that the FDIS is able to detect single and multiple faults, see Fig. 6(c).

As a final remark, results show the practical value of the theoretical proposal. In addition, they show some advantages over other proposals found in literature, such as:

- shorter detection times;
- single and multiple fault isolation without sensor redundancy;
- detection of different kind of faults, including disconnection, progressive, offset and gain faults;
- recovery from a faulty condition.

4.3. Analysis of residuals against disturbances and parameter variations

Simulations were performed in order to analyze the residual levels against parameter and fault variations at different load levels. The FDIS was implemented in MATLAB/Simulink environment based on the block diagram of Fig. 1, with parameters listed in Table 3. A three-phase inverter composed by ideal switches was implemented, using a switching frequency of 10 kHz. All results were obtained with the IM working at rated speed. Only residual from observer $\mathbf{\Sigma}^a$ is analyzed due to the fact both observers presents similar results.

The FDIS was tested against variations of R_s and R_r at load levels 100%, 50% and 10%, without sensor faults. Parameter variations were introduced by modifying the parameters in the IM model as $R_s = R_{s0} + \Delta R_s$ and $R_r = R_{r0} + \Delta R_r$, where subindex 0 denotes rated values, ΔR_s and ΔR_r denotes the variations introduced in stator and rotor resistances, respectively. Peak values of residual ν_a in steady state, denoted by $\nu_{a_{\max}}$, were obtained for each parameter variation.

Figs. 7 and 8 show results of parameters variations. It can be observed that residuals are affected by the variations of both parameters, even in healthy sensor condition. Residual levels caused by variations of R_s are independent of the load level (Fig. 7). In the case of variations of R_r (Fig. 8), residuals increase when the load level is increases. Therefore, errors in the R_r parameter affects

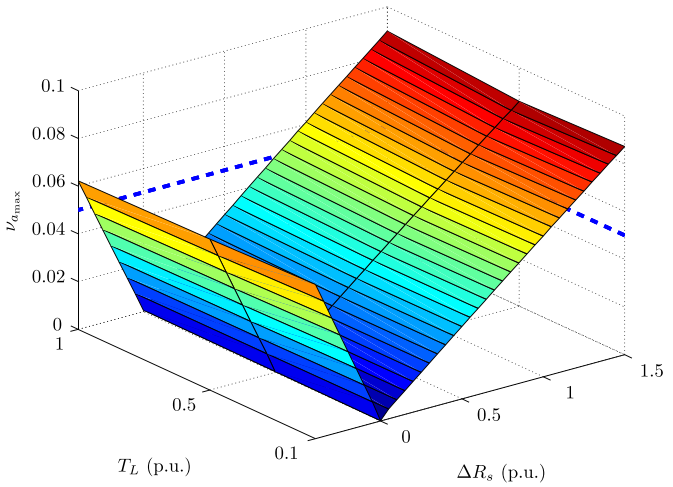

Fig. 7. Maximum residual values under variations of stator resistance at different load levels.

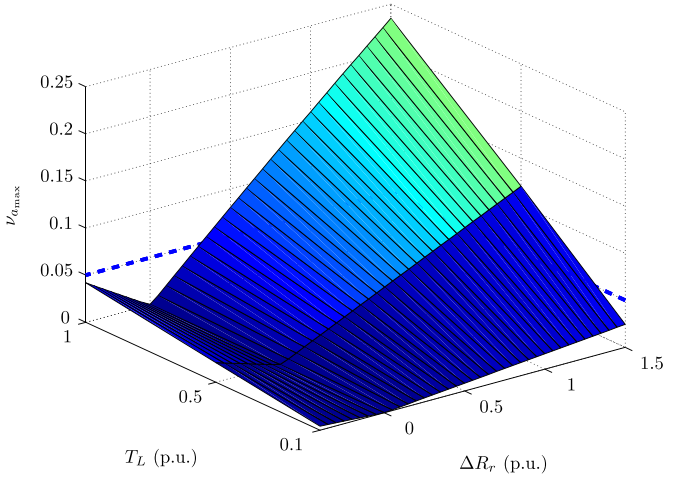

Fig. 8. Maximum residual values under variations of rotor resistance at different load levels.

the decoupling between residuals and the load torque.

Results show that false fault detection may occur in case of parameter variations if threshold levels are not high enough. For example, using the threshold level C_{th} shown in Table 3, a false fault detection could be produced if R_s increases more than 85% or if R_r increases more than 40% of its rated values.

Additionally, peak residual levels in steady state are obtained for different values of the offset-fault signal $m_a = f_0$, with f_0 constant, at the load levels 100%, 50% and 10% (see Fig. 9). Results show that residual levels increase according to de magnitude of the fault signal, independently of the load level. The magnitude of the faults which could be detected by the FDIS depends on the threshold level. For example, using the threshold C_{th} shown in Table 3, offset faults must be higher than 18% of rated phase current in order to be detected by the FDIS. Therefore, results demonstrate that parameter uncertainties and fault levels must be taken into account in order to select the threshold levels.

5. Conclusions

In this paper, current sensor fault detection and isolation (FDI) in induction motor (IM) drives was investigated. In a first step, IM modelling was threated considering a drive with two line current

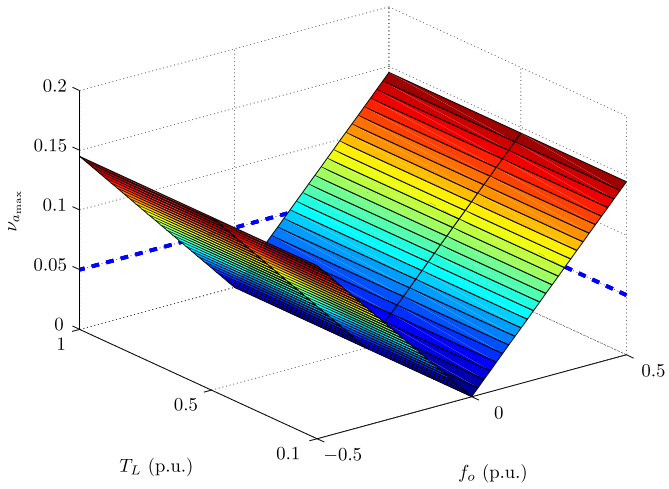

Fig. 9. Maximum residual values under different constant fault signals and load levels.

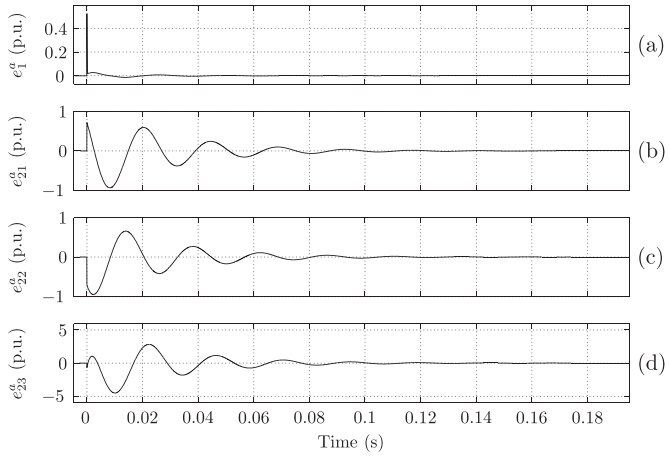

Fig. 10. Transient of estimation errors from observer Σ^a.

sensors prone to arbitrary faults. The geometric approach applied to the proposed IM model representations allowed to establish the detectability of sensor faults, while obtaining a subsystem independent of load torque. Next, it was demonstrated that it is possible to establish the isolability of sensor faults, without the need of redundant sensors. Besides, the applied procedure allowed us to obtain subsystems sensitive to faults in a specific sensor, but independent from faults in the other sensor. From the obtained subsystems, it was possible to build a bank of observers for residuals generation. Such residuals depend on both, the fault signal and its derivative.

Experimental tests demonstrate the feasibility of the addressed design methodology. Results show that different kind of fault are detected and isolated with this proposal, including disconnection, progressive, offset and gain faults. The proposal demonstrates a short detection time as well as the ability to detect single and multiple faults without sensor redundancy. Moreover, the recovery from a faulty condition is demonstrated.

An analysis of residuals against disturbances and parameter variations was performed, demonstrating that these effects must be taken into account in order to select the threshold levels for residuals processing.

Acknowledgment

This work was supported by Universidad Nacional de Río Cuarto (UNRC) and Consejo Nacional de Investigaciones Científicas y Técnicas (CONICET).

Appendix A. Observers performance

In this appendix, the performance of the observers is shown by analyzing simulation results. The bank of observers was implemented in MATLAB/Simulink environment, using the test bench described in Section 4.3. Only observer Σ^a is analyzed due to the fact that both observers show similar results.

Observer Σ^a is started at $t = 0$ s with the IM working at rated operating condition in steady state, without sensor faults. Fig. 10 shows the transient produced in estimation errors ${e_1}^a$ and $\boldsymbol{e}_2^a = [e_{21}^a, e_{22}^a, e_{23}^a]^\top$, corresponding to the estimation errors for SMO and HGO, respectively, after the observer startup. It can be noted that $e_1^a = 0.52$ p.u. at $t = 0$ s and reaches a null level for $t > 0.025$ s, see Fig. 10(a), by considering an estimation error under 0.01 p.u. as a null level. Similarly, $e_{21}^a = 0.71$ p.u. and $e_{22}^a = -0.70$ p.u. at $t = 0$ s, then reach null levels for $t > 0.141$ s, see Fig. 10(b) and (c). In addition, $e_{23}^a = -0.68$ p.u. at $t = 0$ s and reaches a null level after $t = 0.179$ s, see Fig. 10(d). Therefore, results show that all estimation errors tend to zero and have a null levels for $t > 0.179$ s, demonstrating the proper performance of designed observers.

Appendix B. Supplementary data

Supplementary data associated with this paper can be found in the online version at http://dx.doi.org/10.1016/j.conengprac.2016.04.014.

References

Aguilera, F., de la Barrera, P., & De Angelo, C. (2012). Behavior of electric vehicles and traction drives during sensor faults. In *2012 the tenth IEEE/IAS international conference on industry applications (INDUSCON)* (pp. 1–7). Fortaleza, CE, Brazil.

Alwi, H., & Edwards, C. (2014). Development and application of sliding mode LPV fault reconstruction schemes for the ADDSAFE benchmark. *Control Engineering Practice*, *31*(October), 148–170.

Arnanz, R., Miguel, L. J., Perán, J. R., & Mendoza, A. (2011). A modified direct torque control with fault tolerance. *Control Engineering Practice*, *19*(9), 1056–1065.

Bisheimer, G., De Angelo, C., Solsona, J., & Garcia, G. (2008). Sensorless PMSM drive with tolerance to current sensor faults. In *Proceedings of 34th annual conference of IEEE industrial electronics (IECON2008)* (pp. 1379–1384). Orlando, FL, USA, November 2008.

Busawon, K., & De Leon-Morales, J. (2000). An observer design for uniformly observable non-linear systems. *International Journal of Control*, *73*(November (15)), 1375–1381.

Chakraborty, C., & Verma, V. (2015). Current sensor fault detection and isolation technique for induction motor drive using axes transformation. *IEEE Transactions on Industrial Electronics*, *62*(March (3)), 1943–1954.

De Persis, C., & Isidori, A. (2001). A geometric approach to nonlinear fault detection and isolation. *IEEE Transactions on Automatic Control*, *46*(June (6)), 853–865.

Drobnič, K., Nemec, M., Fišer, R, & Ambrožič, V. (2012). Simplified detection of broken rotor bars in induction motors controlled in field reference frame. *Control Engineering Practice*, *20*(8), 761–769.

Du, D., Jiang, B., & Shi, P. (2014). Sensor fault estimation and accommodation for discrete-time switched linear systems. *IET Control Theory Applications*, *8*(July (11)), 960–967.

Espinoza-Trejo, D. R., & Campos-Delgado, D. U. (2009). Detection and isolation of actuator faults for a class of non-linear systems with application to electric motors drives. *IET Control Theory Applications*, *3*(October (10)), 1317–1329.

Fonod, R., Henry, D., Charbonnel, C., Bornschlegl, E., Losa, D., & Bennani, S. (2015). Robust FDI for fault-tolerant thrust allocation with application to spacecraft rendezvous. *Control Engineering Practice*, *42*, 12–27.

Freire, N., Estima, J., & Cardoso, A. (2014). A new approach for current sensor fault diagnosis in PMSG drives for wind energy conversion systems. *IEEE Transactions on Industry Applications*, *50*(March (2)), 1206–1214.

Giantomassi, A., Ferracuti, F., Iarlori, S., Ippoliti, G., & Longhi, S. (2015). Electric motor fault detection and diagnosis by kernel density estimation and Kullback–

Leibler divergence based on stator current measurements. *IEEE Transactions on Industrial Electronics*, *62*(March (3)), 1770–1780.

Khelouat, S., Benalia, A., Boukhetala, D., & Laleg-Kirati, T., (2012). A geometric approach for fault detection and isolation of stator short circuit failure in a single asynchronous machine. In *American control conference 2012* (pp. 5138–5145). Montreal, Canada, June.

Kommuri, S., Rath, J., Veluvolu, K., Defoort, M., & Soh, Y. C. (2015). Decoupled current control and sensor fault detection with second-order sliding mode for induction motor. *IET Control Theory Applications*, *9*(4), 608–617.

Marino, R., Scalzi, S., Tomei, P., & Verrelli, C. (2013). Fault-tolerant cruise control of electric vehicles with induction motors. *Control Engineering Practice*, *21*(June (6)), 860–869.

Mustafa, M. O., Nikolakopoulos, G., Gustafsson, T., & Kominiak, D. (2016). A fault detection scheme based on minimum identified uncertainty bounds violation for broken rotor bars in induction motors. *Control Engineering Practice*, *48* (March), 63–77.

Najafabadi, T., Salmasi, F., & Jabehdar-Maralani, P. (2011). Detection and isolation of speed-, DC-Link voltage-, and current-sensor faults based on an adaptive observer in induction-motor drives. *IEEE Transactions on Industrial Electronics*, *58* (May (5)), 1662–1672.

Pons-Llinares, J., Antonino-Daviu, J., Riera-Guasp, M., Bin Lee, S., Kang, T., & Yang, C. (2015). Advanced induction motor rotor fault diagnosis via continuous and discrete time-frequency tools. *IEEE Transactions on Industrial Electronics*, *62* (March (3)), 1791–1802.

Rahme, S., & Meskin, N. (2015). Adaptive sliding mode observer for sensor fault diagnosis of an industrial gas turbine. *Control Engineering Practice*, *38*(May), 57–74.

Raisemche, A., Boukhnifer, M., Larouci, C., & Diallo, D. (2014). Two active fault-tolerant control schemes of induction-motor drive in EV or HEV. *IEEE Transactions on Vehicular Technology*, *63*(January (1)), 19–29.

Riera-Guasp, M., Antonino-Daviu, J., & Capolino, G. (2015). Advances in electrical machine, power electronic, and drive condition monitoring and fault detection: *State of the art*. *IEEE Transactions on Industrial Electronics*, *62*(March (3)), 1746–1759.

Schuh, M., Zgorzelski, M., & Lunze, J. (2015). Experimental evaluation of an active fault-tolerant control method. *Control Engineering Practice*, *43*(0), 1–11.

Shi, X., & Krishnamurthy, M. (2014). Survivable operation of induction machine drives with smooth transition strategy for EV applications. *IEEE Journal of Emerging and Selected Topics in Power Electronics*, *2*(September (3)), 609–617.

Yu, Yong, Wang, Ziyuan, Xu, Dianguo, Zhou, Tao, & Xu, Rong (2014). Speed and current sensor fault detection and isolation based on adaptive observers for IM drives. *Journal of Power Electronics*, *14*(September (5)), 967–979.

Zhang, J., Zhao, J., Zhou, D., & Huang, C. (2014). High-performance fault diagnosis in PWM voltage-source inverters for vector-controlled induction motor drives. *IEEE Transactions on Power Electronics*, *29*(November (11)), 6087–6099.

Zhang, J., Swain, A., & Nguang, S. (2014). Simultaneous robust actuator and sensor fault estimation for uncertain non-linear Lipschitz systems. *IET Control Theory Applications*, *8*(September (14)), 1364–1374.

Zhang, X., Foo, G., Vilathgamuwa, M., Tseng, K., Bhangu, B., & Gajanayake, C. (2013). Sensor fault detection, isolation and system reconfiguration based on extended Kalman filter for induction motor drives. *IET Electric Power Applications*, *7*(August (7)), 607–617.